

# Matrix-Assisted Energy Conversion in Nanostructured Piezoelectric Arrays

Xianying Wang,<sup>†,‡</sup> Kanguk Kim,<sup>§</sup> Yinmin Wang,<sup>\*,†</sup> Michael Stadermann,<sup>†</sup> Aleksandr Noy,<sup>†,||</sup> Alex V. Hamza,<sup>†</sup> Junhe Yang,<sup>‡</sup> and Donald J. Sirbuly<sup>\*,†,§</sup>

<sup>†</sup>Physical and Life Sciences Directorate, Lawrence Livermore National Laboratory, Livermore, California 94550, United States, <sup>‡</sup>School of Materials Science and Engineering, University of Shanghai for Science and Technology, Shanghai 200093, China, <sup>§</sup>Department of NanoEngineering, University of California, San Diego, La Jolla, California 92093, United States, and <sup>||</sup>School of Natural Sciences, University of California, Merced, California 95343, United States

**ABSTRACT** We demonstrate an organic/inorganic hybrid energy-harvesting platform, based on nanostructured piezoelectric arrays embedded in an environmental-responsive polymer matrix, which can self-generate electrical power by scavenging energy from the environment. A proof of principle device is designed, fabricated, and tested using vertically aligned ZnO nanowires and heat as the local energy source. The device layout takes advantage of the collective stretching motion of piezoelectric ZnO NWs, induced by the shape-change of the matrix polymer, to convert the thermal energy into direct current with output power densities of  $\sim 20$  nW/cm<sup>2</sup> at a heating temperature of  $\sim 65$  °C. The responsive nature of polymeric matrices to various stimuli makes this nanostructured piezoelectric architecture a highly versatile approach to scavenging energy from a multitude of environments including fluid-based and chemical-rich systems.

**KEYWORDS** Energy-conversion, piezoelectric, ZnO, Si, hybrid nanogenerator, Seebeck effect

Encouraging progress has been made recently in the development of nanowire (NW)-based piezoelectric nanogenerators.<sup>1–8</sup> In fact, exciting results from various groups working on ZnO, poly(vinylidene fluoride) (PVDF), barium titanate (BaTiO<sub>3</sub>), and lead zirconate titanate (PZT) have shown device architectures with different powering modes including alternating current (ac)<sup>4–7</sup> and direct current (dc).<sup>9</sup> One key limitation, however, of many piezoelectric-based nanogenerators is the requirement of mechanical energy sources (e.g., mechanical vibration or motion) to generate electrical current. This restricts the use of these nanodevices to a general environment where a direct mechanical energy source is available. To activate the motion of nanopiezoelectric materials through alternate energy sources, such as thermal, photonic, and/or chemical, it will be crucial to investigate new methods of coupling the piezoelectric transducers directly to media that can convert a nonmechanical energy source into piezoelectric strain. This capability will enable materials to be submersed in a variety of environments that have both nontraditional power sources such as mechanical vibrations/motion and pressure gradients as well as traditional power sources such as light, heat, and chemical energy.

In this work, we report a self-powered platform that relies on the response of a polymeric film to drive the piezoelectric effect in a nanowire array. To test the concept of polymer

facilitated mechanical-to-electrical conversion, we chose to study the well-reported ZnO nanowire system that can be grown by different routes including chemical vapor deposition<sup>10,11</sup> or solution-based techniques<sup>12</sup> and embed the NW array in an environmental-responsive organic polymer.<sup>13</sup> In comparison to other ZnO NW-based nanogenerators, the deformation of the ZnO NWs in our devices are not directly induced by external forces, but rather caused by the shape change in the polymer matrix as it responds to external stimuli. With this hybrid approach, the NWs are near uniformly distributed inside the polymer matrix and can deform collectively under stimulation, thus each individual piezoelectric transducer can contribute power to the device. Using a thermal energy source as our test stimulant, we demonstrate that dc electric currents can be generated by the expansion of the polymer matrix with a simple, cheap device architecture. In addition, since our platform utilizes matrix-assisted mechanical-to-electrical conversion, we have the ability to design energy-harvesting structures that are tuned to scavenge energy from a variety of sources including light, heat, pressure, chemical, and mechanical.

A schematic of our nanoconverter (NC) is shown in Figure 1a. An array of vertically aligned ZnO (n-type) NWs is embedded in the environmental-responsive polymer poly(vinyl chloride-co-vinyl acetate-co-2-hydroxypropyl acrylate) (PVC). Vertically aligned ZnO NWs were epitaxially grown on 2 mm × 2 mm a-plane sapphire substrates via a chemical vapor transport and condensation (CVTC) process as described elsewhere.<sup>14</sup> The scanning electron microscopy (SEM) image of the as-grown ZnO NWs (Figure 1b) shows

\* To whom correspondence should be addressed. E-mail: (Y.M.W.) ymwang@llnl.gov; (D.J.S.) dsirbuly@ucsd.edu.

Received for review: 08/12/2010

Published on Web: 11/09/2010

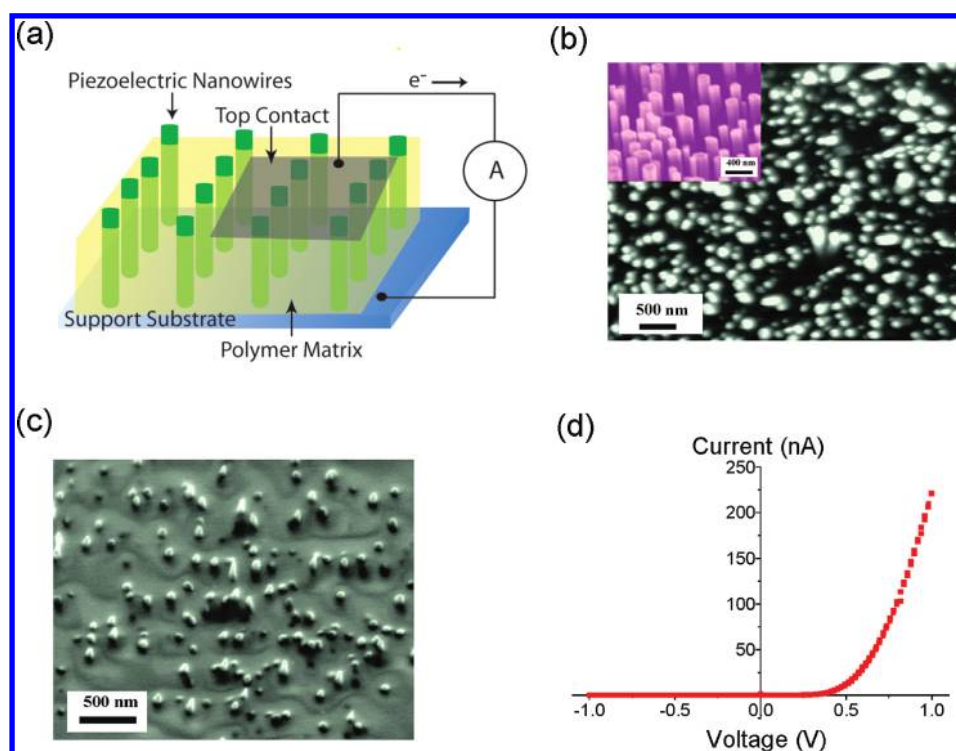


**FIGURE 1.** Design and fabrication of a ZnO-PVC polymer hybrid energy nanoconverter (NC). (a) Schematic of an NC device. (b) Top-view SEM image of the as-grown ZnO NWs on sapphire. The density of the NWs is about  $30/\mu\text{m}^2$ . Inset:  $30^\circ$  tilt view of the vertically aligned ZnO NWs. (c) A SEM image of the nanowire array after infiltrating with the PVC polymer and oxygen plasma etching. About 50% of the NWs are exposed after plasma etching. (d) A characteristic  $I$ - $V$  plot of an NC device showing rectification behavior and a turn-on voltage of  $\sim 400$  mV.

the nanowire diameters ranging from 60–120 nm, lengths between 7–10  $\mu\text{m}$ , and an areal density of  $\sim 30/\mu\text{m}^2$ . After growth, the NW forest was infiltrated by drop-casting a 1% PVC solution (in 1,4-dioxane) on the substrate. The physical and mechanical properties of PVC polymers allow for room-temperature formation of uniform, flexible thin films. After drying the PVC film at room temperature, the top surface was oxygen plasma etched to clean and expose the NW tips for making electrical contacts. A typical SEM image of the exposed NW tips ( $\sim 0.5 \mu\text{m}$  long) is shown in Figure 1c. After etching back a portion of the PVC film, the NW density is measured to be  $\sim 15/\mu\text{m}^2$ , leaving  $\sim 50\%$  of the NWs unexposed. A 200 nm Au/5 nm Ti top contact electrode ( $\sim 1 \text{ mm}^2$  contact area) was deposited via electron beam evaporation. The bottom electrode was defined by placing silver paste on the underlying ZnO thin film that formed during the growth process. The electrical transport characteristics of the nanodevices were tested using a standard electrical probe station (Signatone S-1160) equipped with tungsten micro-manipulator probes, a power source meter (Keithley 2602), and recording software. Figure 1d displays a characteristic  $I$ - $V$  curve of a fabricated NC array that shows the current rectification behavior of the device and a turn on voltage of  $\sim 400$  mV. The electronic barrier formed at the metal–semiconductor (Au–ZnO) interface is a key component in the operation of the device and is discussed in more detail later.

The PVC film has a coefficient of thermal expansion (CTE) of  $70 \times 10^{-6}/\text{K}$  compared to sapphire and ZnO with CTEs

of  $8 \times 10^{-6}/\text{K}$  and  $3 \times 10^{-6}/\text{K}$ , respectively. The substantial CTE mismatch between the substrate and the polymer film can lead to large residual stresses inside the PVC film upon a temperature change/fluctuation. Therefore, a piezoelectric nanowire array embedded in such a polymer matrix should be perturbed by the internal strain within the polymer as the temperature is elevated, providing a direct thermal-to-mechanical-to-electrical transformation in the ZnO NC. We tested this hypothesis by placing a Peltier hot plate underneath the sapphire substrate and thermally stimulating the device. To get a good approximation of the temperature on the top side of the NC device as a function of heating voltage, a small k-type thermal couple was placed on the NC surface and the temperature was recorded at various heating voltages (Figure 2a). A strong short-circuit current on the order of tens of nanoamperes (nA) was observed from the nanodevice (Figure 2b) at various heater voltages. The corresponding open-circuit voltages of the device were also measured (Figure 2c) and showed a direct relationship with temperature. The resistance of the NC remained relatively constant at  $\sim 90 \text{ k}\Omega$  over the narrow heating temperature range we used (see Supporting Information Figure S1). As evident from the short-circuit current and open-circuit voltage traces, there is a slight lag in the recorded values in comparison to the applied voltage to the heater. This lag is likely due to the time it takes heat generated by the Peltier device to transfer through the sapphire/ZnO film and into the polymer as supported by Figure 2a. The stability of the

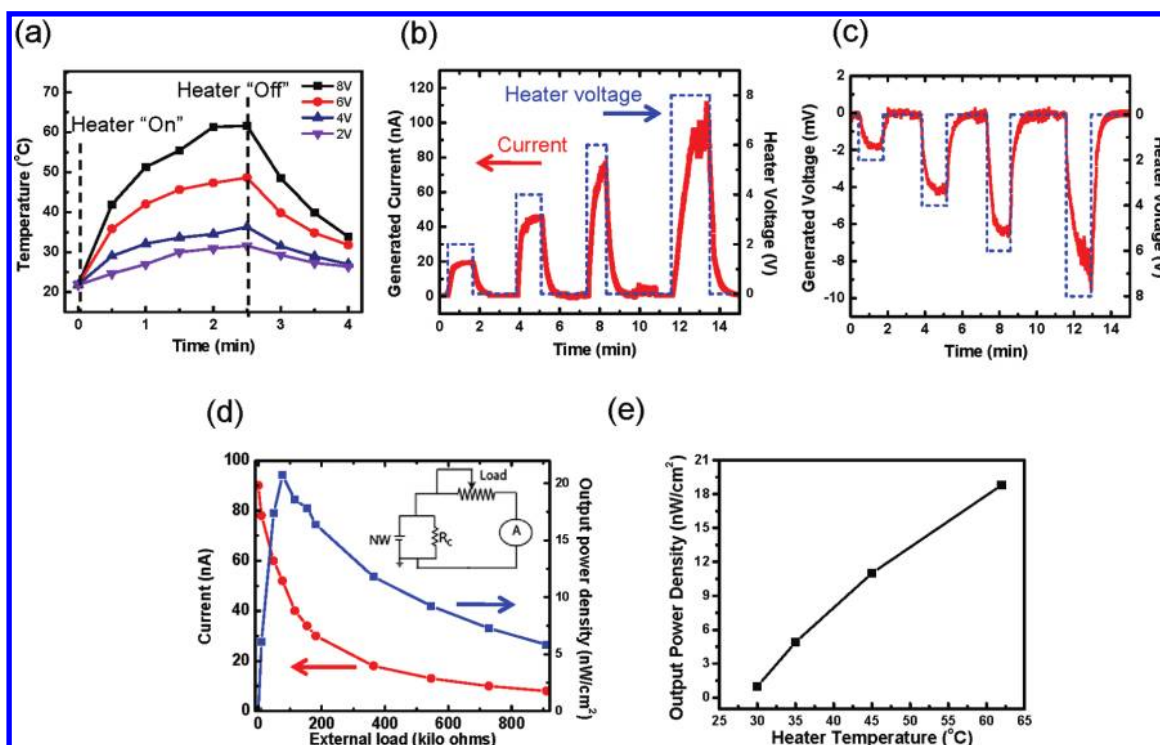


FIGURE 2. Power generation of an NC under thermal stimulation. (a) The temperature profile measured from the top surface of the NC at different Peltier heating voltages. (b) Electric current generated from an NC while heating with the Peltier at voltages of 2, 4, 6, and 8 V (blue dashed lines). (c) Same as (b), but the generated voltage is being plotted. Note that the temperature in the devices does not immediately return back to room temperature [also see plot in (a)] after the Peltier heater is turned off during both voltage and current measurement experiments. (d) The electric current (red trace) and output power density of the nanoconverter (blue trace) when connected to different external loads. A Peltier heating voltage of 8 V ( $\sim 65$  °C) was used for each measurement. A maximum output power density is observed when the external load is close to the internal resistance of  $\sim 90$  k $\Omega$ . (e) The maximum output power by an NC at heating temperatures ranging from room temperature to  $\sim 65$  °C. The maximum output was determined by connecting different loads to an NC device and monitoring the electric current, as seen in (d).

NC devices is also important, specifically how reproducible the peak and baseline current levels are during the “power-up” and “power-down” modes, respectively. We have repeatedly cycled our devices over many hours of operation and have not seen any significant changes in the power output, although continual testing will be necessary to fully understand degradation pathways in the NCs.

To confirm that the electrical signals are generated from the NC device and not an artifact of our experimental setup, we carried out lead exchange experiments on various devices. When the high source and low drain probes were reversed on the electrical contacts of the device, we recorded current levels of similar magnitude but opposite signs (see Supporting Information Figure S2), indicating that the current flow was being driven by the NC and not by residual potentials generated by the measurement electronics. To verify that the electrical circuit setup was not interfering or causing any artificial voltages or current we tested the noise level of the probe station by connecting different external loads (1–500 k $\Omega$ ) in series without the NC device (see Supporting Information Figure S3). Depending on the resistance load, we found that the noise level in the electric current ranged from  $\sim 50$  nA (for 1 k $\Omega$  resistor) to  $\sim 0.1$  nA (for 500 k $\Omega$  resistor) with an upper end in the voltage noise

of  $\sim 50$   $\mu$ V. Therefore, using the measured resistance of  $\sim 90$  k $\Omega$  for our NC device, we predict a noise current contribution of  $<0.6$  nA to our measured values.

The maximum output power from our NC device was measured by connecting different external loads in series. In general, at a given heating temperature the maximum power-output of our NC device was achieved when the external load approximately equals the internal resistance of the device (Figure 2d). The effective contact area determined for a typical NC is  $\sim 1.0$  mm  $\times$  1.0 mm, which yields power density values of 1–19 nW/cm<sup>2</sup> for temperatures ranging from 22–65 °C (Figure 2e). Even though the device configuration and performance are not optimized, the power densities are sufficiently high enough to meet the power requirements to drive many nanowire and nanotubes-based devices used for sensors and other nanoelectronic architectures.<sup>15–18</sup>

The physical working principle of the organic–inorganic hybrid device can be understood based on the piezoelectric behavior of ZnO NWs. The NWs have their *c*-axis oriented perpendicular to the substrate (parallel to growth axis) and produce a piezoelectric field potential when the Zn and O atoms are nonsymmetrically moved due to strain on the crystal. As illustrated in Figure 3a–b, this charge separation

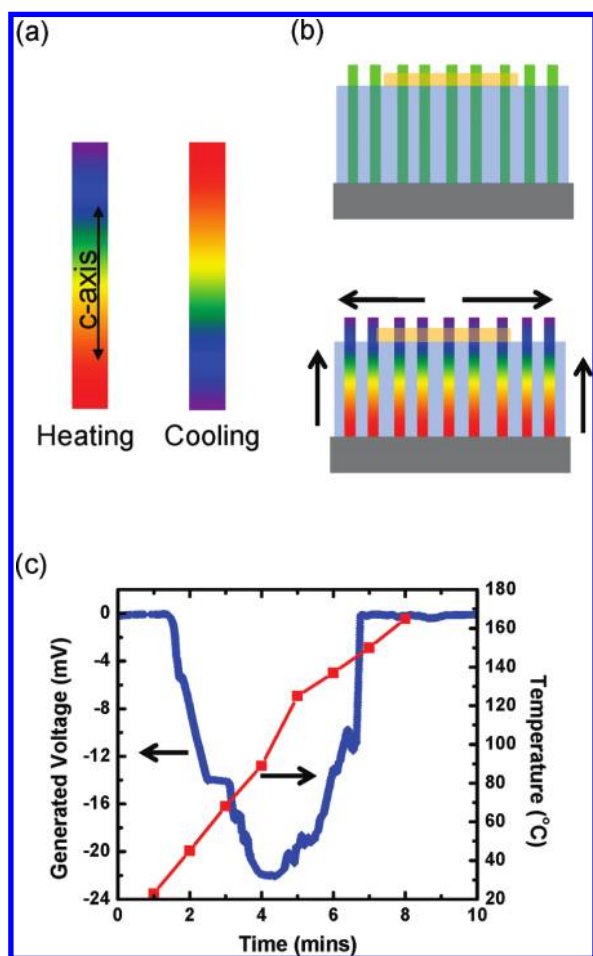


FIGURE 3. Working principle of the NC device. (a) Charge distribution within the ZnO NWs after heating (left) or cooling (right). The blue and red colors indicate a negative and positive potential relative to the ground state, respectively. The bottom of the wire is the interface between the NW and the sapphire substrate. (b) Schematic illustrating the steady-state (top) and thermally agitated (bottom) state of the ZnO NWs embedded in a PVC matrix. As the polymer expands relative to the substrate, a stress along the axis of the NWs is generated. (c) Voltage generated by an NC device heated in an oven from 20 to 165 °C (red symbols). At temperatures above  $\sim 100$  °C, the NC loses its ability to generate power because the PVC undergoes structural relaxation above its glass transition point ( $T_g \sim 65$  °C).

in the ZnO nanowires can be induced by the surrounding polymer matrix, which acts as a pulling handle on the NWs as the polymer expands. Prior to heating, the PVC matrix lies in a steady state (assuming constant ambient temperature), but expands vertically and laterally as thermal energy is added to the system. The polymer is not permitted to expand isotropically because it is supported by the underlying substrate, and therefore subjects the NWs to an axial tensile stress along the *c*-axis. It is possible the NWs also undergo lateral stress that slightly bends the NWs, but this motion is likely a weak contribution to the overall electrical signal. The thin underlying ZnO film on top of the sapphire substrate likely has little impact on the power-generation ability of our devices. Our electrical current measurements (i.e., direction of current flow) shown in Figure 2a–c indicate

that the tops of the ZnO wires (at the polymer–metal contact interface) become increasingly negative as the temperature rises and are positively charged at the other end (Figure 3a). Note that the initial electronic state of the ZnO surfaces (e.g., the side surface), which could influence the polarity of the top and bottom portions of NWs, may be generated by the oxygen plasma treatment used to expose the NW tips.<sup>19</sup>

From a first-order approximation (see Supporting Information), without considering the polarization and dielectric screening effect, the electric potential ( $U$ ) created during tension can be calculated from  $U = [A_p E_p / (A_p E_p + A_{nw} E_{nw})] \times [(\alpha_p - \alpha_{nw}) \Delta T \times (L_{nw} / d_{33})]$ , where  $E_p$  is the Young's modulus of PVC (2900–3300 MPa),<sup>20</sup>  $E_{nw}$  is Young's modulus of ZnO ( $\sim 100$  GPa),  $\alpha_p$  is the thermal expansion coefficient of PVC ( $\sim 70 \times 10^{-6}$  /K),  $\alpha_{nw}$  is the expansion coefficient of ZnO ( $\sim 3 \times 10^{-6}$  /K) along the *c*-axis,<sup>21,22</sup>  $L_{nw}$  is the NW length ( $\sim 5 \mu\text{m}$ ),  $\Delta T$  is the change of the temperature,  $d_{33}$  is the piezoelectric constant ( $\sim 14.3$ – $26.7$  pm/V) of a ZnO NW along the *c*-axis,<sup>23</sup> and  $A_p$  and  $A_{nw}$  are the cross-sectional area fractions of the polymer and nanowire, respectively. This idealized expression suggests that the maximum piezoelectric output voltage for a PVC matrix can be in the range of a few volts, but experimentally we observe values around 10 mV. Among the factors that influence the output potentials include the free carrier density of the ZnO NWs (which creates a screening effect and reduces electric potentials) and the nature of the Schottky barrier (which affects the charge separation).<sup>24</sup> As expected, for a softer polydimethylsiloxane (PDMS) polymer (see below) the strain is predicted to be about 3 orders of magnitude lower. The lateral expansion of the PVC polymer, which can induce bending in the NWs, can also generate charge separation across the lateral direction leading to positive or negative potentials on the side surfaces of the NWs.<sup>3</sup> However, as the side surface of the NW tips is in constant contact with the Au electrode, the fields generated by the displacement of  $\text{Zn}^{2+}$  and  $\text{O}^{2-}$  ions are immediately neutralized. As a result, the contribution of the bending motion to the overall piezoelectric effect of our NC is expected to be small and can generally be ignored.

To better understand the nature of the polymer-induced tensile strain in the piezoelectric nanowires, we replaced the PVC matrix with a softer polydimethylsiloxane (PDMS) polymer. The small Young's modulus of PDMS (0.36–0.87 MPa), compared to PVC (2900–3300 MPa),<sup>20</sup> should produce a weaker tensile strain, assuming similar adhesion interactions between the polymer and semiconductor, on the ZnO nanowires even though the CTE of PDMS ( $310 \times 10^{-6}$ /K)<sup>25</sup> is higher than PVC ( $70 \times 10^{-6}$ /K). Both polymers have high electrical resistivities ( $\sim 10^{15}$   $\Omega\text{cm}$ ) and low thermal conductivities ( $< 0.2$  W/m·K) leading to similar electrical insulation and temperature gradients across the polymer film. Under similar heating conditions ( $\sim 50$  °C) the PVC infiltrated NC produces about a 20-fold higher current level than the ZnO arrays filled with PDMS (see Supporting

Information Figure S4). In addition, if the polymer matrix is removed without disrupting the contacts, no signal is generated (see Supporting Information Figure S5). Both of these controls help support a piezoelectric driven power and validate that the polymer matrix has a significant effect on the output properties of the NC devices.

As noted above, the energy barrier created at the metal–semiconductor interface is important in our mechanism for current generation. Given that the work functions of Au and Ag are 5.1 and 4.2 eV, respectively, the electron affinity ( $E_a$ ) of ZnO is 4.5 eV, and without considering the near-surface state effects<sup>26,27</sup> the top Au–ZnO interface likely forms a Schottky-type barrier compared to the more ohmic bottom contact. The entire electric transport mechanism described in Figure 1a is therefore controlled by the top Au–ZnO interface. When the negatively charged top surface (generated during tensile stress) is connected to the Au contact, the Au–ZnO interface is forward biased and electric current flows across the interface. Likewise, when the top surface is positively charged (generated under compression), the Au–ZnO interface is reverse biased and little electric current will flow across the junction. The strong self-generated electric current (Figure 2b) and direction of electron flow supports this hypothesis. The model of the nanowire motion depicted in Figure 3a,b also suggests that the vertical alignment and Schottky contacts are key factors to generating dc power. As the PVC matrix begins to expand and exert stress on the NWs, a piezoelectric potential is generated along the nanowire axis due to the polarization of the  $\text{Zn}^{2+}$  and  $\text{O}^{2-}$  ions in the crystal. Because of the Schottky-like interface and slow neutralization of the strain field in the nanowire, the piezoelectric potential can exist for long periods of time (tens to hundreds of seconds).<sup>26,28</sup> It is likely that our piezoelectric potential, given the slow deformation time of the polymer, is significantly reduced during the thermal experiments. Indeed, replacing the thermoplastic matrix with faster responding matrices would be a direct route to enhance the performance of our NC devices. As the ZnO nanowires are strained by the expanding polymer, electrons begin to flow across metal–semiconductor junctions where the piezoelectric potential is high enough to overcome the interfacial energy barrier. This process can continue for long periods of time (minutes to hours) given the large number of metal–semiconductor energy barriers present across the nanowire array. Our dc signal is therefore due to a collective contribution of independent nanowires discharging as the strain induced piezoelectric potential overcomes the local interfacial energy barriers between the nanowire and metal contact.

Since the PVC polymer used has a nominal glass transition temperature ( $T_g$ ) of  $\sim 65$  °C,<sup>29</sup> it is expected that a device infiltrated with PVC will lose its ability to harvest thermal energy at temperatures above  $T_g$  due to the structural relaxation and/or conformational changes in the polymer. To test the operational temperature range of the NC, we

continuously heated a device from room temperature to 165 °C in a furnace while monitoring its output performance. Figure 3c displays the oven temperature and the output voltage signals from the NC device as a function of time. The plot illustrates that the output voltage signal (blue trace) reaches its maximum ( $-22$  mV) at  $\sim 100$  °C before dropping sharply down to zero after 145 °C. The rapid drop off in the voltage is presumably due to the onset of structural relaxation within the polymer matrix as the glass transition temperature is reached. Interestingly, after cooling the NC device back to room temperature, we found that the nano-device no longer had the same capability to convert thermal energy into electric current (see Supporting Information Figure S6). This is likely due to the ZnO NWs detaching from the substrate during the heating process or degradation in the metal-semiconductor interfaces.

The PVC polymer used in these experiments is a sufficient thermal insulator (thermal conductivity  $\sim 0.19$  W/m K), and it is anticipated that thermal gradients will form across the polymer film as well as locally around the ZnO nanowires. To get a better understanding of the thermal gradient across the polymer film, we measured the temperature at the top of the polymer surface and the top of the ZnO thin film (Figure 4a) using small ( $<0.5$  mm) k-type thermocouples. Since the as-grown ZnO nanowires are n-type semiconductors, the temperature gradient along the  $c$ -axis invokes a negative and positive electric potential on the top and bottom surfaces, respectively, suggesting that the potentials we observed in Figure 2c could be the contribution of both piezoelectric and thermoelectric effects. To differentiate the thermoelectric from the piezoelectric potential, we homogeneously heated (i.e., the top and bottom sides of the device have the same temperature) a device to about 42 °C in a furnace, thus minimizing any temperature gradients across the polymer film. As illustrated in Figure 4b, the isothermally heated NC device produced an output potential that was about 0.4 mV less than the potential produced with a similar device heated from the backside only (Figure 2c). At 42 °C, under Peltier heating, the temperature gradient between the top and bottom surface of the polymer (Figure 4a) is  $\sim 6$  K. The average Seebeck coefficient ( $S = -dV/dT$ , where  $dV$  is the thermoelectric potential, and  $dT$  is the temperature gradient) of the ZnO NWs is thus estimated to be  $-67$   $\mu\text{V/K}$ , assuming the temperature gradient of the ZnO NWs is the same as that of the polymer. However, since the thermal conductivity of the ZnO NWs ( $3$ – $10$  W/m K)<sup>30</sup> is substantially higher than that of PVC, the estimated Seebeck coefficient value is likely an upper limit. This value is reasonably smaller than high performance thermoelectric materials such as  $\text{Bi}_2\text{Te}_3$  ( $-287$   $\mu\text{V/K}$ , n-type). Comparing the output performance of the isothermally and bottom-heated devices suggests that over 94% of the electric potential generated comes from the piezoelectric contributions.<sup>31</sup>

Further supporting data comes from control runs using nonpiezoelectric silicon nanowire arrays (see Supporting In-

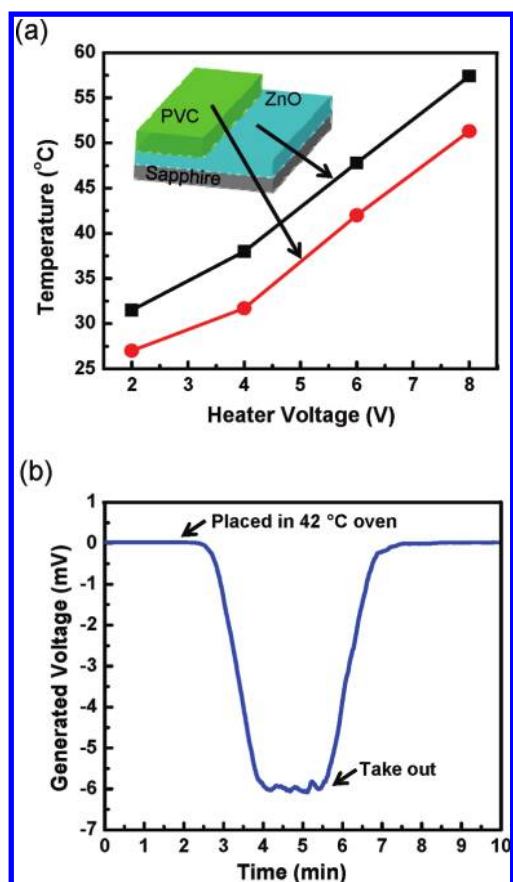


FIGURE 4. Thermoelectric contribution in an NC device. (a) Temperatures measured at the top and bottom of the polymer. The temperature was recorded after heating the device for 1 min. The estimated heating rate of the device is 0.23 °C/s. (b) The voltage generated from an isotropically heated (42 °C) NC device. The maximum voltage is  $\sim 0.4$  mV lower than a device heated from the bottom.

formation Figure S7). Silicon nanowire arrays were synthesized via an electroless etching approach<sup>32</sup> which resulted in nanowires with dimensions similar to the ZnO nanowire arrays ( $\sim 100$  nm diameters; 10  $\mu$ m lengths). As evident from the short-circuit traces (see Supporting Information Figure S7), very small currents are generated from a Si nanowire array infiltrated with PVC. The measurable current output likely stems from a thermoelectric effect that has recently been reported for silicon nanowires.<sup>33,34</sup> The dominance of the piezoelectric contribution is also supported by the elevated (above  $T_g$ ) heating (Figure 3e) and the polymer exchange experiments (see Supporting Information Figure S4).

In summary, we have demonstrated an energy conversion platform that utilizes nanostructured piezoelectrics embedded in an environmental-responsive polymer matrix to convert thermal energy into electrical power. The device architecture does not require elaborate top contacts or electrodes to produce dc power as the output relies on the collective discharging of individual transducers with different metal–semiconductor energy barriers. Since our transduction mechanism is driven by the material coupled to the piezoelectrics, we can tailor the infiltrating matrix and device

design so that power can be scavenged from various energy sources including light, mechanical, pressure, fluids, and/or chemical. These promising results demonstrate the effectiveness of a matrix-assisted piezoelectric nanoenergy converter and highlight the unique attributes of environmental-responsive coatings in creating multifunctional nanopower devices and sensors.

**Acknowledgment.** The authors thank A. B. Artyukhin and T. S. Wilson for stimulating discussions. D.J.S. acknowledges funding from the Graboske fellowship while at LLNL and University of California, San Diego start-up funds under his current appointment. X.Y.W. and J.H.Y. are supported by China 973 program (2010CB234609), Shanghai NanoProject (1052 nm03000), NSFC (51072119), and Shanghai Rising Star Program (09QA1404100). A.N. was supported by the U.S. Department of Energy, Office of Basic Energy Sciences, Division of Materials Sciences and Engineering. This work was performed in part under the auspices of the U.S. Department of Energy by Lawrence Livermore National Laboratory under Contract DE-AC52-07NA27344.

**Supporting Information Available.** Piezoelectric potential due to matrix-assisted strain: first-order approximation, deformation strain rates of the ZnO nanowires at different heater voltages, Table S1, and additional figures. This material is available free of charge via the Internet at <http://pubs.acs.org>.

## REFERENCES AND NOTES

- Lieber, C. M.; Wang, Z. L. *MRS Bull.* **2007**, *32*, 99–108.
- Qin, Y.; Wang, X. D.; Wang, Z. L. *Nature* **2008**, *451*, 809–U5.
- Wang, Z. L.; Song, J. H. *Science* **2006**, *312*, 242–246.
- Wang, Z. Y.; Hu, J.; Suryavanshi, A. P.; Yum, K.; Yu, M. F. *Nano Lett.* **2007**, *7*, 2966–2969.
- Xu, S.; Qin, Y.; Xu, C.; Wei, Y.; Yang, R.; Wang, Z. L. *Nat. Nanotechnol.* **2010**, *5*, 366–373.
- Chang, C. E.; Tran, V. H.; Wang, J. B.; Fuh, Y. K.; Lin, L. W. *Nano Lett.* **2010**, *10*, 726–731.
- Qi, Y.; Jafferis, N. T.; Lyons, K.; Lee, C. M.; Ahmad, H.; McAlpine, M. C. *Nano Lett.* **2010**, *10*, 524–528.
- Service, R. F. *Science* **2010**, *328*, 304–305.
- Wang, X. D.; Song, J. H.; Liu, J.; Wang, Z. L. *Science* **2007**, *316*, 102–105.
- Yang, P. D.; Yan, H. Q.; Mao, S.; Russo, R.; Johnson, J.; Saykally, R.; Morris, N.; Pham, J.; He, R. R.; Choi, H. J. *Adv. Funct. Mater.* **2002**, *12*, 323–331.
- Yao, B. D.; Chan, Y. F.; Wang, N. *Appl. Phys. Lett.* **2002**, *81*, 757–759.
- Greene, L. E.; Yuhas, B. D.; Law, M.; Zitoun, D.; Yang, P. D. *Inorg. Chem.* **2006**, *45*, 7535–7543.
- Schmaljohann, D. *Adv. Drug Delivery Rev.* **2006**, *58*, 1655–1670.
- Huang, M. H.; Wu, Y. Y.; Feick, H.; Tran, N.; Weber, E.; Yang, P. D. *Adv. Mater.* **2001**, *13*, 113–116.
- Bachtold, A.; Hadley, P.; Nakanishi, T.; Dekker, C. *Science* **2001**, *294*, 1317–1320.
- Chopra, S.; McGuire, K.; Gothard, N.; Rao, A. M.; Pham, A. *Appl. Phys. Lett.* **2003**, *83*, 2280–2282.
- Huang, Y.; Duan, X. F.; Cui, Y.; Lauhon, L. J.; Kim, K. H.; Lieber, C. M. *Science* **2001**, *294*, 1313–1317.
- Patolsky, F.; Zheng, G.; Hayden, O.; Lakadamyali, M.; Zhuang, X.; Lieber, C. M. *Proc. Natl. Acad. Sci. U.S.A.* **2004**, *101*, 14017–14022.
- Ay, M.; Nefedov, A.; Girol, S. G.; Woll, C.; Zabel, H. *Thin Solid Films* **2006**, *510*, 346–350.
- Ogorkiewicz, R. M. *Engineering properties of thermoplastics: A collective work produced by Imperial Chemical Industries Ltd., Plastics Division*; Wiley: New York, 1970.

- (21) Albertsson, J.; Abrahams, S. C.; Kvik, A. *Acta Crystallogr., Sect. B* **1989**, *45*, 34–40.
- (22) Ibach, H. *Phys. Status Solidi* **1969**, *33*, 257–265.
- (23) Zhao, M. H.; Wang, Z. L.; Mao, S. X. *Nano Lett.* **2004**, *4*, 587–590.
- (24) Wang, Z. L. *Adv. Mater.* **2009**, *21*, 1311–1315.
- (25) CTE data available at <http://www.dowcorning.com> (accessed Mar 2010).
- (26) Liu, J.; Fei, P.; Song, J. H.; Wang, X. D.; Lao, C. S.; Tummala, R.; Wang, Z. L. *Nano Lett.* **2008**, *8*, 328–332.
- (27) Mosbacher, H. L.; Strzemechny, Y. M.; White, B. D.; Smith, P. E.; Look, D. C.; Reynolds, D. C.; Litton, C. W.; Brillson, L. J. *Appl. Phys. Lett.* **2005**, *87*, No. 012102.
- (28) Zhou, J.; Fei, P.; Gao, Y. F.; Gu, Y. D.; Liu, J.; Bao, G.; Wang, Z. L. *Nano Lett.* **2008**, *8*, 2725–2730.
- (29) <http://www.sigmaaldrich.com/catalog/search/ProductDetail/ALDRICH/388033> (accessed Feb 2010).
- (30) Kulkarni, A. J.; Zhou, M. *Appl. Phys. Lett.* **2006**, *88*, 141921.
- (31) Gao, Y.; Wang, Z. L. *Nano Lett.* **2007**, *7*, 2499–2505.
- (32) Peng, K. Q.; Yan, Y. J.; Gao, S. P.; Zhu, J. *Adv. Mater.* **2002**, *14*, 1164–1167.
- (33) Boukai, A. I.; Bunimovich, Y.; Tahir-Kheli, J.; Yu, J. K.; Goddard, W. A.; Heath, J. R. *Nature* **2008**, *451*, 168–171.
- (34) Hochbaum, A. I.; Chen, R. K.; Delgado, R. D.; Liang, W. J.; Garnett, E. C.; Najarian, M.; Majumdar, A.; Yang, P. D. *Nature* **2008**, *451*, 163–167.